Dynamic coupling on the design of space structures

Andrés García-Pérez[a, *], Ángel Sanz-Andrés[a], Gustavo Alonso[a], Marcos Chimeno Manguán[b]

[a] Instituto Universitario de Microgravedad "Ignacio Da Riva" (IDR/UPM), Escuela Técnica Superior de Ingeniería Aeronáutica y del Espacio (ETSIAE), Universidad Politécnica de Madrid, Pza. Cardenal Cisneros 3, 28040 Madrid, Spain

[b] Escuela Técnica Superior de Ingeniería Aeronáutica y del Espacio (ETSIAE), Universidad Politécnica de Madrid (UPM), Pza. Cardenal Cisneros 3, 28040 Madrid, Spain

*Corresponding author: andres.garcia.perez@upm.es
angel.sanz.andres@upm.es
gustavo.alonso@upm.es
marcos.chimeno@upm.es

Abstract

For the design of space structures, the dynamic coupling between equipment and the satellite (or between a satellite and the launcher) is usually avoided due to negative effects like high stresses produced by structural resonance. The usual procedure to assure the dynamic decoupling is by limiting the minimum value of natural frequency of the secondary structure to a value high enough above the main natural frequencies of the main structure. However, in some spacecraft configurations, it is unavoidable that some parts or equipment present natural frequencies close to the main natural frequencies of the spacecraft because these parts may be massive or may have a special interface design with low stiffness. This dynamic coupling provokes modifications on the modal behavior of the satellite, which can lead to a significant decrease in the first natural frequency of the entire satellite. To analyze this phenomenon, a representative but simple mathematical model is studied to evaluate the influence of the design parameters of space structures. Analytical expressions are obtained that can help to highlight the influence of the parameters. The results are demonstrated with the example of the UPMSat-2 satellite design.

Keywords: 2-DOF, dynamic coupling, natural frequency, modal analysis, space structures, UPMSat-2

Nomenclature

Symbol	Description	Units
$[K]$	Stiffness matrix	
$[M]$	Mass matrix	
$\{J\}$	Response to a static displacement at the base	
f_{10}	Maximum first natural frequency of the system	Hz
f_{20}	Natural frequency of the isolated secondary mass	Hz
f_i	Natural frequency i of the system	Hz
f_{min}	Required minimum natural frequency of the system	Hz
f_r	Reference natural frequency of the system	Hz
K	Stiffness constant of the main structure	N/m
k	Stiffness constant of the secondary part	N/m
M	Large or primary mass	kg
m	Small or secondary mass	kg
$M_{eff,i}$	Modal effective mass of the i mode	kg
$m_{eff,i}$	Modal effective mass fraction of the i mode	
q_{ij}	Component j of the eigenvector i	
u_i	Displacement coordinate	m
x_i	Dimensionless eigenvalue i of the system	

Greek symbol	Description	Units
$\{\phi_i\}$	Eigenvector of mode i	
α	Stiffness ratio	
β	Mass ratio	
Γ_i	Ancillary parameter	
μ	Frequency ratio or tuning parameter	
φ	Ratio between f_{min} and f_{10}	
ω_{10}	Maximum first natural circular frequency of the system	rad/s
ω_{20}	Natural circular frequency of the isolated secondary mass	rad/s
ω_i	Natural circular frequency i of the system	rad/s
ω_r	Reference natural circular frequency of the system	rad/s

Subscript	Description
i	Mode of the system
j	Component of the eigenvector

1 Introduction

The phenomenon of the dynamic or modal coupling is of great interest in the design of space structures. The usual procedure in the space industry is to avoid the dynamic coupling between the launcher with its carried satellites, or between a satellite and its equipment. The principal purpose is to prevent the adverse effects that appear when the frequency range of the dynamic loads generated during the launch phase and other events like landing, testing or ground operations, coincide with the main natural frequencies of the structures, provoking the phenomenon of structural resonance, which leads to high stresses and forces and the generation of undesirable structural damages [1, 2].

To avoid the structural resonance of the satellite at the low frequency vibrations generated by the launch vehicle, the launcher authority specifies minimum limit values for both lateral and longitudinal natural frequencies of the satellite [2]. In a similar way, the satellite designers specify minimum values for the natural frequencies for their payloads and equipment to assure that they are high enough above the fundamental natural frequencies of the satellite. The main reason is to protect the equipment by avoiding the structural resonance with the dynamic loads transmitted through the structure of the satellite, where the frequencies of the highest acceleration amplitudes at the equipment interface correspond to the natural frequencies of the satellite. Another reason is to avoid the undesirable effects caused by the modal coupling with the main structure of the satellite, which can put at risk the structural integrity of the whole system. Usually for early design phases, a fixed minimum frequency requirement on the secondary structure is defined by the primary structure designer. This approach provides on many occasions a very restrictive requirement that leads to oversized designs for the secondary part. In some space projects, particular components like large deployable antennas or massive instruments with low stiff attachment cannot be designed to have the first natural frequency higher enough than the main natural frequencies of the satellite due to the difficulty of achieving the necessary increase in stiffness. For this reason, a better understanding of the effects of modal coupling is needed to improve the design parameters of this type of space structure.

Different investigations have dealt with the problem of modal coupling in space structures. The importance of the modal coupling between parts on large space structures has been described by Bertram [3], indicating its influence on the attitude dynamics and on the structural response during the launch phase. In [4], the shock specification by a Shock Response Spectrum (SRS) envelope is generated by considering a coupled system representing the secondary and the primary structure. The resulting specification is more realistic than that calculated from the usual procedure of considering both parts decoupled. To provide more precise input loads generated during the launch phase, the coupled load analysis (CLA) is the most recommended way to derive the dynamic loads specification for the satellite [2]. In CLA simulations, a model composed of the finite element model (FEM) of the launcher and a reduced model of the satellite is considered, and in this way, the influence of modal coupling between launcher and satellite is taken into account for more realistic environments. Different approaches to correlate reduced models of satellites have been presented in [5-7] to have more accurate results in CLA. In [8, 9], the low stiffness attachment of a spacecraft with a vibration isolation system is studied. This type of mechanical interface configuration has the advantage of reducing the levels of vibrations that are transmitted to the spacecraft, but the drawback of decreasing the main natural frequencies of the attached spacecraft to the same frequency range as the modes of the launcher.

Therefore, the dynamic coupling between spacecraft and launcher cannot be neglected with this type of interface design.

The modal coupling is also of relevance to the attitude dynamics of spacecraft. The dynamic coupling between the large deployable antenna typically used in communications satellites and the rest of spacecraft is taken into account in [10] to study the attitude dynamics of the entire satellite. This type of payload constitutes a non-negligible mass with a low stiff joint with the satellite after deployment, which leads to a local natural frequency of the same order of magnitude as those of the global modes of the satellite. The modal coupling should also be taken into account to derive a reliable simulation during the mechanical tests [11].

To have a better understanding of the influence of the main parameters on the results of a coupled system, a 2 degree of freedom (2-DOF) system has been widely used in numerous research papers. Frahm [12] introduced the concept of the tuned mass damper (TMD) and Den Hartog [13] studied its effects, where the secondary mass is suited to have a natural frequency similar to the main mode of the system. TMD has been applied in civil engineering to reduce the amplitude of response vibrations of buildings subjected to aerodynamic or earthquake loads [14-18]. In recent years, the concept of TMD has been improved leading to the creation of more sophisticated devices with better performance and effectiveness [19]. In [20], analytical solutions are calculated to find the best position and the optimal damping constants to minimize the vibrations on flexible structures. Semi-active vibration absorbers (SVA) used in conjunction with TMD to control the performance in order to be adapted to the disturbing frequency in real-time are studied in [21, 22]. In [23], a semi-active TMD with resettable variable stiffness (RVS-TMD) is proposed to improve the performance of the existing TMD systems. In [24], a TMD with variable inertance is numerically studied to include the effects of different parameters in the performance of a wide range of forcing frequencies. Shape memory alloys (SMA) can be employed as TMD for seismic mitigation [25]. Other designs with the same approach are the tuned liquid mass damper (LTMD) [26], the tuned liquid column gas damper [27], the magnetically tuned mass damper [28], the magnetorhelogical damper with semi-active TMD [29, 30] and the piezoelectric vibration energy harvesting beam as a TMD [31].

TMD concept has also been applied in the space industry. The use of TMDs have been preferred in space industry due to their simplicity and the possibilities that they offer for reducing the response due to particular modes. In [32], TMDs are employed to reduce the oscillations of printed circuit boards (PCB) during vibration loads, being more efficient than increasing the thickness. In [33], the dynamic analysis of space structures with multiple tuned mass dampers (MTMD) is enhanced with formulations of the reverberation matrix method (RMM). In [34], the location and design of TMD devices to improve the performance of space mirrors is evaluated, showing that by means of an eddy current damper a great reduction in the response can be achieved (up to 80%) depending on the TMD location, damping and targeted modes. In [35], a semi-active control system consisting of variable-friction dampers linked to the structure with cables is proposed and studied. In [36], a new mode decomposition method for structures with non-classical damping and very closely distributed modes is proposed and verified with a 2-DOF system with a tuned mass damper (TMD).

The majority of these research works about TMD [12-36] have focused on the reduction of the amplitude of oscillations of the main structure, and in some of them [16] also on the decrease of generated forces and stresses. But some aspects such as the decrease of the natural frequencies

of the entire system and the modification of the mode shapes and the modal effective masses have not been studied in depth yet. These aspects are fundamental in the structural design of space structures, especially when modal coupling cannot be avoided. Therefore, the purpose of this paper is to present a parametric study of modal coupling using an undamped 2-DOF system in section 2. The main results such as the natural frequencies, eigenvectors and modal effective mass fractions are expressed with analytical equations to evaluate the influence of the design parameters. These analytical expressions are applied in the optimization of the structural design in section 3. The paper is focused in the case of a satellite as the main structure and an equipment or payload as the secondary part. From a satellite design point of view, the objective is to guarantee the structural integrity of the entire satellite, which can be in serious risk depending on the design of a particular component, even if the mass of this component is seemingly negligible compared to the mass of the rest of the satellite. The analytical expressions are compared with the FEM results for the design of the structural lateral panels of the university-class microsatellite UPMSat-2 in section 4. Finally, conclusions are drawn in section 5.

2 Mathematical model

The 2-DOF model considered for the entire spacecraft is shown in Fig. 1. The spacecraft main body (mass M) is fixed to the launcher through the separation system whose stiffness can be modeled as a spring of constant K.

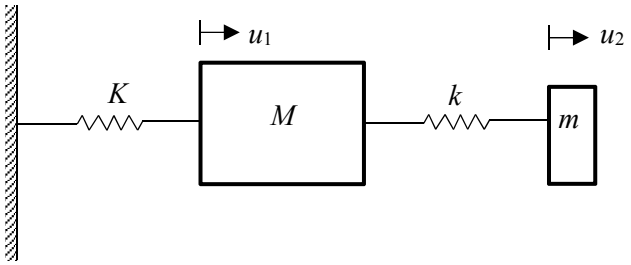

Figure 1: Frahm absorber. M, m; K, k; u_1, u_2: masses, stiffness and absolute displacements of the whole spacecraft and a small loosely fixed part, respectively.

In the spacecraft, a small part (a panel, radiator, instrument, etc.) with a small mass, m, is mounted with a weaker mechanical interface (spring constant $k << K$). This configuration is denoted as a "Frahm absorber" and dates back to 1909 [12]. The model is assumed undamped in order to obtain analytical solutions that can be used for a fast estimation of the coupled response as will be shown in the following sections. In space structures, the usual damping values are low (below 5% of the critical damping factor), and it is considered that the damped natural frequencies of a system can be assumed to be the undamped natural frequencies [1, 2]. The analytical results obtained will also apply for systems with proportional damping in terms of the natural frequencies and eigenvectors, and also for the coupled resonances for low damping values.

The aim of this analysis is to study the influence of the design parameters such as the stiffness ratio $\alpha = k/K$ and mass ratio $\beta = m/M$ on the 2-DOF system dynamics (resonant frequencies, eigenmodes, modal effective mass, etc.). Let us define the reference natural frequency (the resonant frequency of the case $m = 0$) $\omega_r^2 = K/M$, the natural frequency of the secondary mass in case of being isolated $\omega_{20}^2 = k/m$, and the dimensionless eigenvalue i of the system $x_i = (\omega_i/\omega_r)^2$.

The equations that describe the dynamics are

$$M\ddot{u}_1 + Ku_1 + k\left(u_1 - u_2\right) = 0 \tag{1a}$$

$$m\ddot{u}_2 + k\left(u_2 - u_1\right) = 0 \tag{1b}$$

Using complex variable notation, $\{q\} = \{q_0\}\,\mathrm{e}^{\mathrm{i}\omega t}$, the system (1) can be written as

$$\left(-\omega^2\begin{bmatrix}1 & 0\\ 0 & \beta\end{bmatrix} + \omega_r{}^2\begin{bmatrix}1+\alpha & -\alpha\\ -\alpha & \alpha\end{bmatrix}\right)\{q_0\} = \{0\} \tag{2}$$

The characteristic equation is

$$\begin{vmatrix}-x+1+\alpha & -\alpha\\ -\alpha & -\beta x+\alpha\end{vmatrix} = 0 \tag{3}$$

and defining $\mu = \dfrac{\alpha}{\beta} = \dfrac{k}{m}\dfrac{M}{K} = \dfrac{\omega_{20}{}^2}{\omega_r{}^2} = x_{20}$ as the tuning parameter, the quadratic equation to calculate the eigenvalues is given by

$$x^2 - x\left(1+\mu\beta+\mu\right) + \mu = 0 \tag{4}$$

The exact solutions of Eq. (4) are

$$x_{1,2} = \frac{1}{2}\left[1+\mu\left(1+\beta\right) \mp \sqrt{\left(1-\mu\right)^2 + \mu\beta\left(2+2\mu+\mu\beta\right)}\right] \tag{5}$$

where the subscripts “1” and “2” indicate the lowest and the highest eigenvalues respectively.

The variations of the dimensionless eigenvalues x_1 and x_2 are shown in Fig. 2 as a function of the tuning parameter μ for different values of mass ratio β below unity, and in Fig. 3 as a function of the mass ratio β, for different constant values of μ. The curves for constant values of the mass ratio β shown in Fig. 2 converge asymptotically to the straight lines $x_i = 1$ and $x_i = \mu$ for $\beta << 1$.

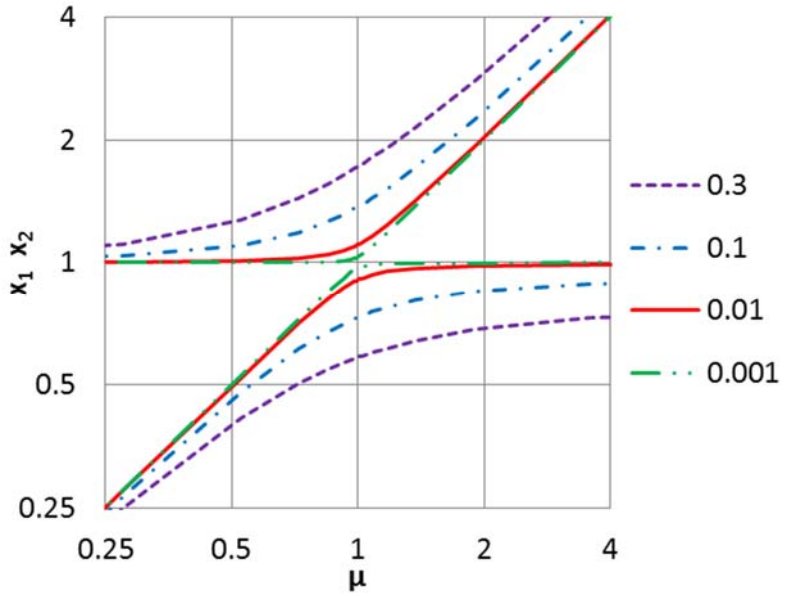

Figure 2: Variation of the dimensionless eigenvalues x_1 and x_2 ($x_1 < 1$; $x_2 > 1$) as a function of the tuning parameter, μ. Legend: values of the mass ratio, β.

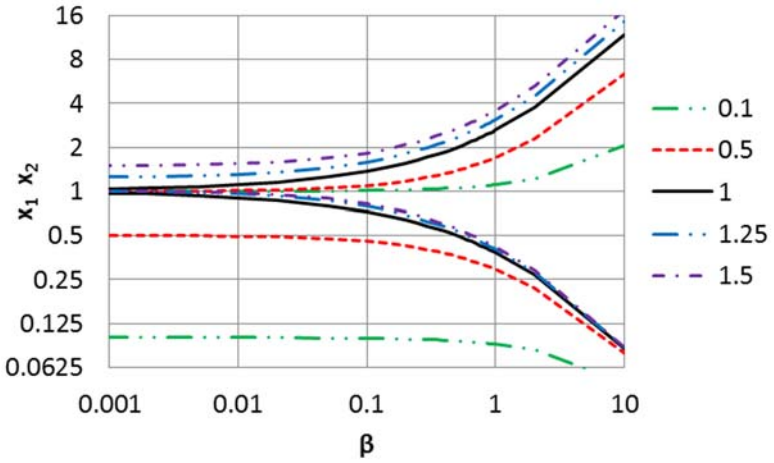

Figure 3: Variation of the dimensionless eigenvalues x_1 and x_2 ($x_1 < 1$; $x_2 > 1$) as a function of the mass ratio, β. Legend: values of the tuning parameter μ.

If the tuning parameter is small, $\mu << 1$, then the natural frequency of the small part alone is much lower than the reference natural frequency and the first mode x_1 corresponds to the motion of this small part, which in first approximation is $x_1 \approx \mu = x_{20} << 1$. The second mode corresponds to the motion of the rest of the structure and its value is close to the reference value ($x_2 \approx 1$). When the tuning parameter μ takes values much larger than unity, $\mu >> 1$, the first mode corresponds to the motion of the entire structure and its value tends asymptotically to $x_{10} = 1 / (1 + \beta)$, which is the maximum value that can take the first dimensionless eigenvalue. This value is obtained when the rigidity between both masses k is very high and the structure can be considered as a single degree of freedom (SDOF) system with stiffness K and a total mass $M + m$. The second mode x_2 is in this case the motion of the small part and its value tends asymptotically to $\mu\ (1 + \beta)$.

The proposed approach can be compared with other methods used for the estimations of the natural frequencies of an undamped 2-DOF system, such as Dunkerley's approach and Rayleigh's quotient [1].

The Dunkerley's method can estimate the first natural frequency of a 2-DOF system by considering the following assumption

$$\omega_{1,Dunk}{}^2 = \frac{1}{\sum_{k=1}^{2} g_{kk} m_{kk}} \tag{6}$$

where, for the considered 2-DOF system,

$$\begin{aligned} &m_{11} = m; && m_{22} = M \\ &g_{11} = \frac{1}{k} + \frac{1}{K} = \frac{k+K}{kK}; && g_{22} = \frac{1}{K} \end{aligned} \tag{7}$$

By using the dimensionless parameters defined in this section, the Dunkerley's estimation for the first dimensionless eigenvalue is given by

$$x_{1,Dunk} = \frac{\omega_{1,Dunk}{}^2}{K/M} = \frac{\mu}{1+\mu+\mu\beta} \tag{8}$$

For the estimation of the first eigenvalue of a 2-DOF system by the Rayleigh's quotient [1], the static response of the system is assumed to be a close estimation of the first eigenvector leading to the following expression of the dimensionless eigenvalue in terms of the design parameters defined in this paper

$$x_{1,Ray} = \frac{\omega_{1,Ray}{}^2}{K/M} = \frac{1}{K/M} \frac{\{\phi\}_1{}^T [K] \{\phi\}_1}{\{\phi\}_1{}^T [M] \{\phi\}_1} = \frac{\mu\beta + (\mu+\mu\beta)^2}{\beta(1+\mu+\mu\beta)^2 + (\mu+\mu\beta)^2} \tag{9}$$

The variation of the first dimensionless eigenvalue x_1 as a function of the tuning parameter μ calculated using the exact analytical method proposed in this paper and compared with the solutions estimated by Dunkerley's and Rayleigh's approaches is shown in Fig. 4. The variations of x_1 as functions of the mass ratio β calculated by using these three methods are compared in Fig. 5.

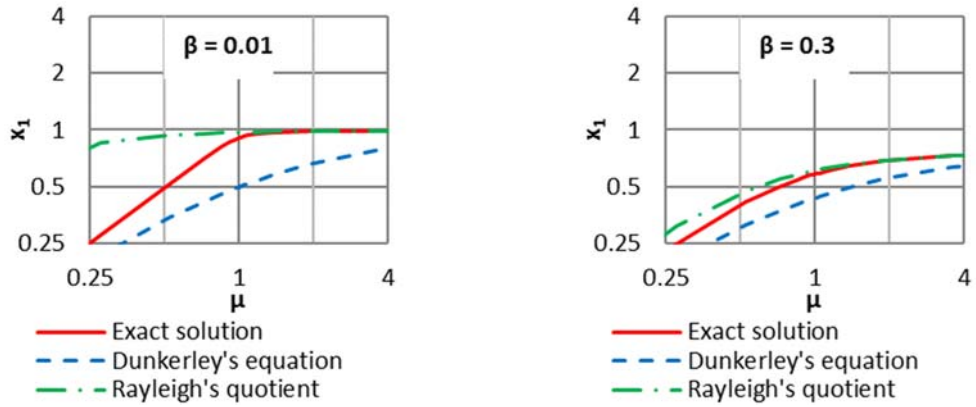

Figure 4: Variation of the dimensionless eigenvalue x_1 as a function of tuning parameter, μ obtained by means of the exact analytical solution, Dunkerley's equation and Rayleigh's quotient for different values of the mass ratio, β.

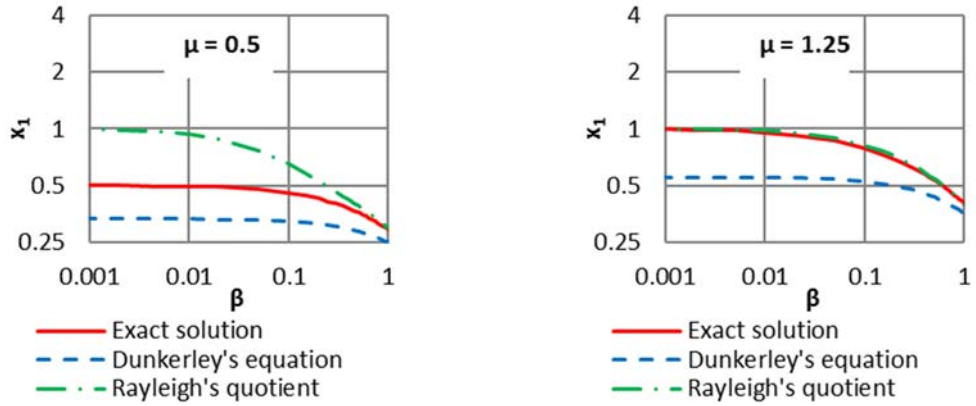

Figure 5: Variation of the dimensionless eigenvalue x_1 as a function of mass ratio, β obtained by means of the exact analytical solution, Dunkerley's equation and Rayleigh's quotient for different values of the tuning parameter, μ.

As can be seen from these plots, the differences of the solutions with Dunkerley's method and Rayleigh's quotient with respect to the exact solutions are noticeable for some ranges of values of the design parameters β and μ. The Dunkerley's method gives values for the first eigenvalue below the exact solution for all range of values of mass ratio β and tuning parameter μ, where the highest differences appear for $\mu = 1$. These differences decrease when β increases. Whereas the Rayleigh's quotient provides results for the first eigenvalue above the exact solution, showing a good agreement for $\mu > 1$, but with higher differences for $\mu < 1$. As for the Dunkerley's method, the difference with the exact solution decreases when the value of the mass ratio β increases.

The advantage of the 2-DOF model developed in this paper is that the solutions are exact for all range of values of β and μ, and the expression (5) used to calculate these solutions is not more complicated than the expressions obtained from Dunkerley's method (Eq. (8)) and from Rayleigh's quotient (Eq. (9)).

In this study, the range of interest for the tuning parameter μ corresponds to values close to unity, where the phenomenon of dynamic coupling between both masses becomes more relevant. The first case considered is for $\mu = 1$. Using Eq. (5), the eigenvalues are given by

$$x_{1,2} = 1 + \frac{\beta}{2} \mp \sqrt{\beta}\sqrt{1 + \frac{\beta}{4}} \tag{10}$$

For small values of the mass ratio $\beta << 1$, and neglecting *O(β)* terms, these dimensionless eigenvalues and the frequencies ratio can be approximated as

$$x_{1,2} \approx 1 \mp \sqrt{\beta}; \qquad \frac{f_{1,2}}{f_r} \approx 1 \mp \frac{1}{2}\sqrt{\beta} \tag{11}$$

Both solutions are slightly smaller and larger, respectively, than the zero order solution $x = 1$. The separation between these frequencies depends on the mass ratio β, and is given by

$$\sqrt{x_2} - \sqrt{x_1} \approx \sqrt{1 + \sqrt{\beta}} - \sqrt{1 - \sqrt{\beta}} \simeq 1 + \frac{1}{2}\sqrt{\beta} - \left(1 - \frac{1}{2}\sqrt{\beta}\right) = \sqrt{\beta} \tag{12}$$

Therefore, the influence of the secondary mass on the natural frequencies of the system is higher than expected a priori. For instance, for a mass ratio $\beta = 0.01$, the frequency separation is $\sqrt{\beta} = 0.1$.

In this range both dimensionless eigenvalues x_1 and x_2 are close to 1, and to find out which is more important in the global response of the entire structure when is excited by its base, it is necessary to calculate the modal effective mass for each mode. As a previous step, the eigenvectors are obtained to know the motion of the masses in both modes.

2.1 Eigenvectors

The eigenvectors describe the motion of both masses for each mode and are calculated from Eq. (2)

$$\{\phi\}_i = \left(q_{i1}, q_{i2}\right)^T \tag{13}$$

Whichever of the two equations obtained can be used to determine the eigenvectors. The election is a matter of analytical simplicity

$$\frac{q_{i2}}{q_{i1}} = \frac{-x_i + 1}{\mu\beta} + 1 \tag{14a}$$

$$\frac{q_{i2}}{q_{i1}} = \frac{\mu}{\mu - x_i} \tag{14b}$$

To have an expression that relates the ratio of eigenvectors components with both the mass ratio β and the dimensionless eigenvalues x_i, the following expression, obtained directly from Eq. (4), is necessary as a previous step

$$\frac{x_i}{\mu} = 1 - \frac{x_i}{1 - x_i}\beta \tag{15}$$

and combining this expression with Eq. (14b), the following equation to determine the eigenvectors is obtained

$$\frac{q_{i2}}{q_{i1}} = \frac{\mu}{\mu - x_i} = \frac{1}{1 - x_i/\mu} = \frac{1 - x_i}{x_i \beta} \tag{16}$$

The explicit expressions of the eigenvectors components as a function of the mass ratio β and the tuning parameter μ are obtained by substituting Eq. (5) in Eq. (14a)

$$\frac{q_{12}}{q_{11}} = \frac{-x_1 + 1}{\mu\beta} + 1 = \frac{1}{2\mu\beta}\left[1 - \mu(1-\beta) + \sqrt{(1-\mu)^2 + \mu\beta(2 + 2\mu + \mu\beta)}\right] \tag{17a}$$

$$\frac{q_{22}}{q_{21}} = \frac{-x_2 + 1}{\mu\beta} + 1 = \frac{1}{2\mu\beta}\left[1 - \mu(1-\beta) - \sqrt{(1-\mu)^2 + \mu\beta(2 + 2\mu + \mu\beta)}\right] \tag{17b}$$

The following expressions are approximations of the detuned ($|\mu - 1| = O(1)$) and the tuned ($\mu = 1$) cases for small values of mass ratio ($\beta << 1$). For the detuned case, the approximated solutions are

For $\mu >> 1$

$$x_1 \approx 1 - \frac{\mu}{\mu - 1}\beta \approx 1 - \beta; \qquad x_2 \approx \mu + \frac{\mu^2}{\mu - 1}\beta \approx \mu(1 + \beta) \tag{18a}$$

$$\frac{q_{12}}{q_{11}} \approx \frac{\mu}{\mu - 1} \approx 1 + \frac{1}{\mu}; \qquad \frac{q_{22}}{q_{21}} \approx -\frac{\mu - 1}{\mu\beta} \approx -\frac{1}{\beta} \tag{18b}$$

For $\mu << 1$

$$x_1 \approx \mu - \frac{\mu^2}{1 - \mu}\beta; \qquad x_2 \approx 1 + \frac{\mu}{1 - \mu}\beta \tag{19a}$$

$$\frac{q_{12}}{q_{11}} \approx \frac{1 - \mu}{\mu\beta}; \qquad \frac{q_{22}}{q_{21}} \approx -\frac{\mu}{1 - \mu} \tag{19b}$$

The eigenvectors are shown in Fig. 6. In the case $\mu >> 1$, the amplitudes of oscillation of the two masses are similar in the first mode. The small mass accompanies the motion of the large mass, in phase for the lower frequency mode, while for the higher mode, large oscillation amplitude motion appears as $\beta << 1$, but 180º out of phase. In the case $\mu << 1$, in the lower frequency mode the oscillation amplitude of the small mass is large, while in the higher frequency mode, the amplitude of the motion of both masses is quite similar, but 180º out of phase.

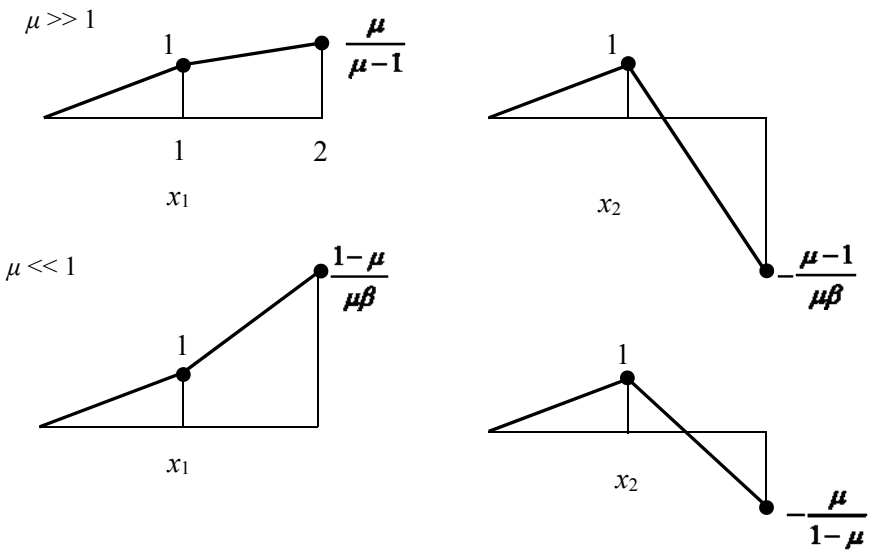

Figure 6: Eigenvectors associated to eigenvalues x_1 and x_2 respectively for detuned case ($\mu \neq 1$).

For the tuned case, $\mu = 1$, the eigenvectors components have the following relationship obtained by substituting Eq. (10) in Eq. (14b):

$$\frac{q_{i2}}{q_{i1}} = \frac{1}{1-x_i} = \frac{1}{-\frac{\beta}{2} \pm \sqrt{\beta}\sqrt{1+\frac{\beta}{4}}} \tag{20}$$

As a first approximation, considering low mass ratios $\beta << 1$, the relationship between the eigenvectors components becomes

$$\begin{aligned} \frac{q_{12}}{q_{11}} &\approx \frac{1}{\sqrt{\beta}} \\ \frac{q_{22}}{q_{21}} &\approx -\frac{1}{\sqrt{\beta}} \end{aligned} \tag{21}$$

As for the detuned case, in the lowest frequency mode both motions are in phase and at the highest frequency mode both motions are 180º out of phase, as are shown in Fig. 7. The amplitude of the small mass motion is much larger ($1/\sqrt{\beta}$) in both modes than that of the spacecraft. This configuration has the same effects as the TMD studied in several works [12-36], where the amplitudes of the main structure are reduced at the expense of the high amplitudes on the secondary mass. But in the problem studied in this paper, these high amplitudes can be dangerous for the equipment represented by the small mass because they can generate excessive stresses and forces above the allowable limits. Therefore, this condition must be carefully studied taking into account this risk for the secondary part.

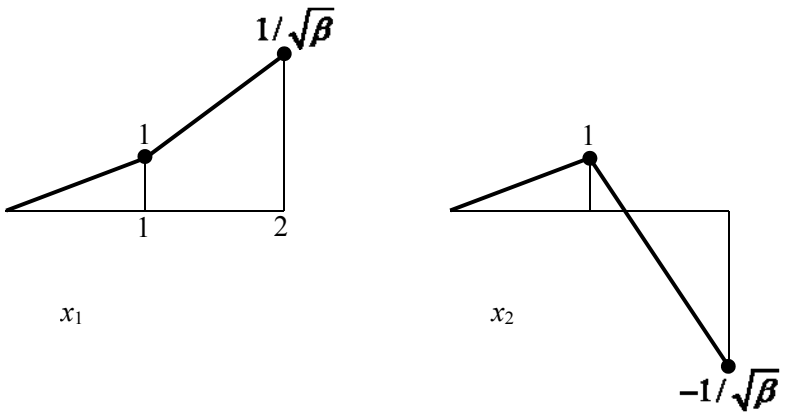

Figure 7: Eigenvectors associated to eigenvalues x_1 and x_2 for the tuned condition case ($\mu = 1$).

2.2 Modal effective mass

To analyze the modal response of a system, the effective mass is a parameter often used. The effective mass fraction is the percentage of total mass participating in the motion of the respective eigenmode. This parameter is a measure to identify the importance of each mode on the global response of a system when it is excited at its base. High values of modal effective masses give high values of interface forces. The expression to calculate the modal effective mass from the mass matrix, the eigenvector and the response to a static displacement at the base is

$$M_{eff,i} = \frac{\left(\{\phi\}_i^T [M]\{J\}\right)^2}{\{\phi\}_i^T [M]\{\phi\}_i} \tag{22}$$

where $\{J\} = (1,1)^T$ is the response to a static displacement at the base. The modal effective mass fraction ($m_{eff,i}$) of the 2-DOF system in this work is given by

$$m_{eff,i} = \frac{M_{eff,i}}{M+m} = \frac{M}{M+m} \frac{\left(1+\beta \frac{q_{i2}}{q_{i1}}\right)^2}{1+\beta\left(\frac{q_{i2}}{q_{i1}}\right)^2} \tag{23}$$

This parameter can be expressed in different ways as a function of the 3 parameters (x_i, β and μ) by combining Eq. (23) with Eqs. (14a) and (14b)

$$m_{eff,i} = \frac{1}{1+\beta} \frac{\left(\mu+\mu\beta-x_i\right)^2}{\left[\left(\mu-x_i\right)^2+\beta\mu^2\right]} = \frac{1}{1+\beta}\left[1+\beta\mu\frac{\beta\mu+\mu-2x_i}{\left(\mu-x_i\right)^2+\beta\mu^2}\right] =$$
$$= 1-\frac{\beta}{1+\beta}\frac{x_i^2}{\left(\mu-x_i\right)^2+\beta\mu^2} \tag{24}$$

Different expressions are given below that relate the modal effective mass fraction as a function of only two independent parameters.

Using Eq. (15) and the first term of Eq. (24), the expressions of $m_{eff,i}$ as a function of the two independent parameters β and x_i is obtained

$$m_{eff,i} = \frac{\beta}{1+\beta} \frac{\left[1+\left(\frac{1-x_i}{x_i}\right)\right]^2}{\left[\beta+\left(\frac{1-x_i}{x_i}\right)^2\right]} = \frac{\beta}{1+\beta} \frac{1}{\left[\beta x_i^{\,2}+\left(1-x_i\right)^2\right]} \tag{25}$$

From Eq. (25), the explicit expression of the dimensionless eigenvalue x_i as a function of $m_{eff,i}$ and β is

$$x_i = \frac{1}{1+\beta}\left[1 \mp \sqrt{\beta \frac{1-m_{eff,i}}{m_{eff,i}}}\right] \tag{26}$$

The equation that relates the modal effective mass fraction $m_{eff,i}$ with the tuning parameter μ and the dimensionless eigenvalue x_i is calculated by substituting the mass ratio β parameter of Eq. (25) with the Eq. (15)

$$m_{eff,i} = \frac{1}{1+\frac{x_i^3}{\mu}\frac{\left(1-x_i\right)}{\left(\mu-x_i\right)}} \tag{27}$$

And finally, to provide the explicit expression of $m_{eff,i}$ as a function of β and μ, the ancillary parameter Γ_i is defined as

$$\Gamma_i \equiv \sqrt{\beta \frac{1-m_{eff,i}}{m_{eff,i}}} \tag{28}$$

From Eq. (15), the tuning parameter μ can be expressed as a function of the modal effective mass fraction $m_{eff,i}$ and β

$$\mu = \frac{1}{\frac{1}{x_i}-\frac{\beta}{1-x_i}} = \frac{1}{\frac{1+\beta}{1-\Gamma_i}-\frac{\beta\left(1+\beta\right)}{\beta+\Gamma_i}} = \frac{\left(1-\Gamma_i\right)\left(\beta+\Gamma_i\right)}{\Gamma_i\left(1+\beta\right)^2} \tag{29}$$

$$\mu = \frac{\left(1-\sqrt{\beta\frac{1-m_{eff,i}}{m_{eff,i}}}\right)\left(\beta+\sqrt{\beta\frac{1-m_{eff,i}}{m_{eff,i}}}\right)}{\sqrt{\beta\frac{1-m_{eff,i}}{m_{eff,i}}}\left(1+\beta\right)^2} \tag{30}$$

The parameter Γ_i can be expressed as an explicit function of the mass ratio β and the tuning parameter μ by solving the following quadratic equation defined from Eq. (29)

$$\Gamma_i^2 + \Gamma_i\left[\mu(1+\beta)^2 - 1 + \beta\right] - \beta = 0 \tag{31}$$

The results are

$$\Gamma_i = \frac{1}{2}\left[1-\beta-\mu(1+\beta)^2 \mp (1+\beta)\sqrt{(1-\mu)^2 + \mu\beta(2+2\mu+\mu\beta)}\right] \tag{32}$$

Finally, the modal effective mass fractions as a function of β and μ are calculated by considering Eqs. (32) and (28)

$$m_{eff,1} = \frac{\beta}{\beta+\Gamma_1^2} = \frac{\beta}{\beta+\frac{1}{4}\left[1-\beta-\mu(1+\beta)^2 + (1+\beta)\sqrt{(1-\mu)^2+\mu\beta(2+2\mu+\mu\beta)}\right]^2} \tag{33a}$$

$$m_{eff,2} = \frac{\beta}{\beta+\Gamma_2^2} = \frac{\beta}{\beta+\frac{1}{4}\left[1-\beta-\mu(1+\beta)^2 - (1+\beta)\sqrt{(1-\mu)^2+\mu\beta(2+2\mu+\mu\beta)}\right]^2} \tag{33b}$$

The variation of the modal effective mass fraction, $m_{eff,i}$ as a function of the dimensionless eigenvalue x_i is shown in Fig. 8. Solid lines are obtained from Eq. (25) for different constant values of the mass ratio β, while dashed lines represent the functions of Eq. (27) for different constant values of μ. A change of behavior is observed in Fig. 8(a) for the curves of constant μ of the first mode, where for $\mu < 1$, each curve decreases monotonously to zero, while for $\mu > 1$, each curve presents a minimum value of $m_{eff,1}$, which is larger than 0.5. This indicates that, for the range of the tuning parameter μ above unity, the first mode always has more modal effective mass, and therefore, more influence on the generated interface forces than the second mode, when a forced acceleration is applied at the system base. This behavior is also observed in Fig. 8(c) for the second mode, with the difference in this case that corresponds to maximum values of the modal effective mass fraction.

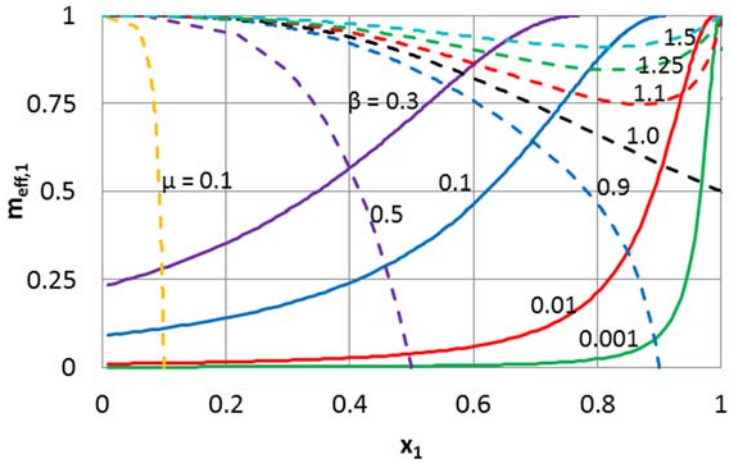

(a) First mode

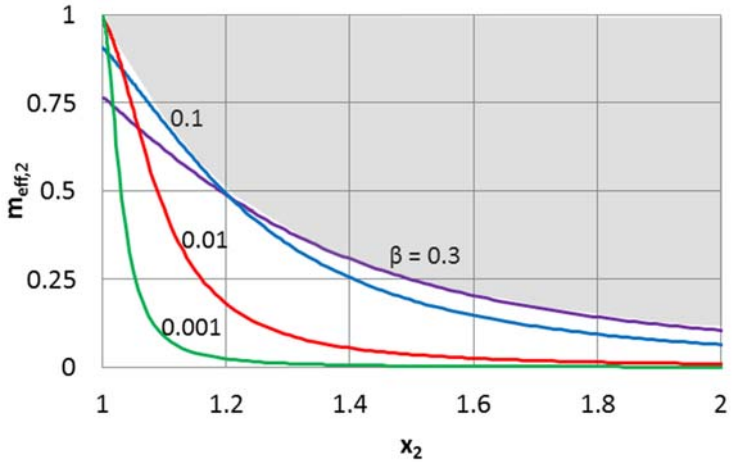

(b) Second mode

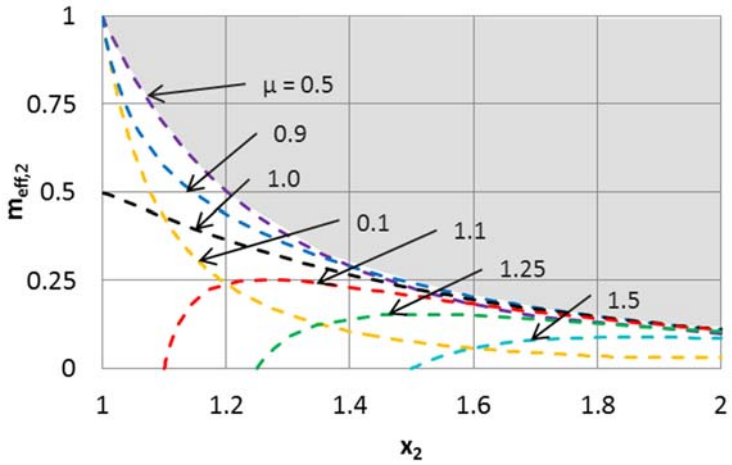

(c) Second mode

Figure 8: Variation of modal effective mass fractions $m_{eff,1}$ and $m_{eff,2}$ as a function of the dimensionless eigenvalues x_1 and x_2. Constant values of the mass ratio β, solid lines. Constant values of the tuning parameter μ, dashed lines. (a) First mode. (b) and (c) Second mode; the solutions only cover the non-shaded area.

For the second mode, the solutions only cover the non-shaded area in the Figs. 8(b) and 8(c). The curve that delimits this area is determined by the calculation of the value of the tuning parameter $\mu_{meff,max}$ that maximizes the modal effective mass fraction of the second $m_{eff,2}$ for a given x_2. This value is obtained from Eq. (27)

$$\frac{\partial m_{eff,2}}{\partial \mu} = 0; \quad \mu_{meff,max} = \frac{x_2}{2} \tag{34}$$

And substituting Eq. (34) in Eq. (27), the formula that defines the border line of the shaded are in Figs. 8(b) and 8(c) is

$$m_{eff,2,max} = \frac{1}{1-4x_2\left(1-x_2\right)} \tag{35}$$

The expression of Eq. (33a) is plotted in Fig. 9 in curves for different constant values of mass ratio β, while the same solutions are shown in Fig. 10 in a graph $m_{eff,i} - \beta$ with curves of constant values of μ.

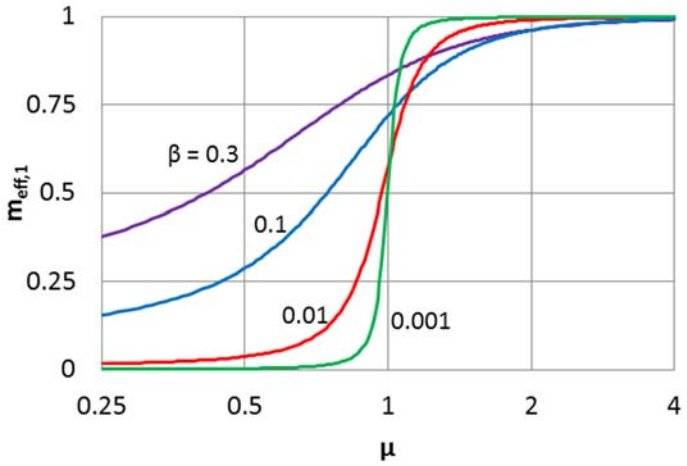

Figure 9: Variation of the modal effective mass fraction, $m_{eff,1}$ as a function of tuning parameter μ. The values of the mass ratio β are indicated.

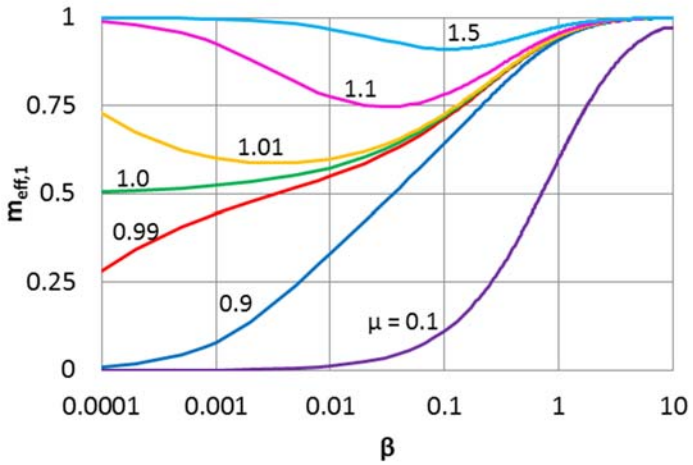

Figure 10: Variation of the modal effective mass fraction, $m_{eff,1}$ as a function of mass ratio, β. The values of the tuning parameter μ are indicated.

As can be seen in Fig. 9, the curves of $m_{eff,1}$ as a function of the tuning parameter μ increase monotonically from $\beta / (1 + \beta)$, which is the ratio between the small mass and the total mass obtained as a solution of Eq. (33a) for $\mu = 0$ (low stiffness joint, $k << 1$), towards unity for $\mu >> 1$, which corresponds to the motion of the entire system.

With the aim of determining the design regions where each mode has more modal effective mass than the other one, it is necessary to calculate the values of μ and β where both modal effective mass fractions are equal to 0.5 and therefore where both modes have the same influence on the global response of the system. This condition leads to the following expression obtained from Eq. (28)

$$\Gamma_1^2 = \Gamma_2^2 = \beta \tag{36}$$

And introducing this value in Eq. (31), the following relationship between μ and β is obtained

$$1 - \beta - \mu(1+\beta)^2 = 0; \quad \mu_{0.5} = \frac{1-\beta}{(1+\beta)^2} \tag{37}$$

Interestingly, this value is always $\mu_{0.5} < 1$. The dimensionless eigenvalues are obtained in this case by combining Eqs. (37) and (5)

$$x_i = \frac{1 \mp \sqrt{\beta}}{1+\beta} \tag{38}$$

The design region where the first mode has more modal effective mass than the second mode ($m_{eff,1} > m_{eff,2}$) corresponds to the zone B indicated in Fig. 11. The boundary that separates both regions is given by Eq. (37).

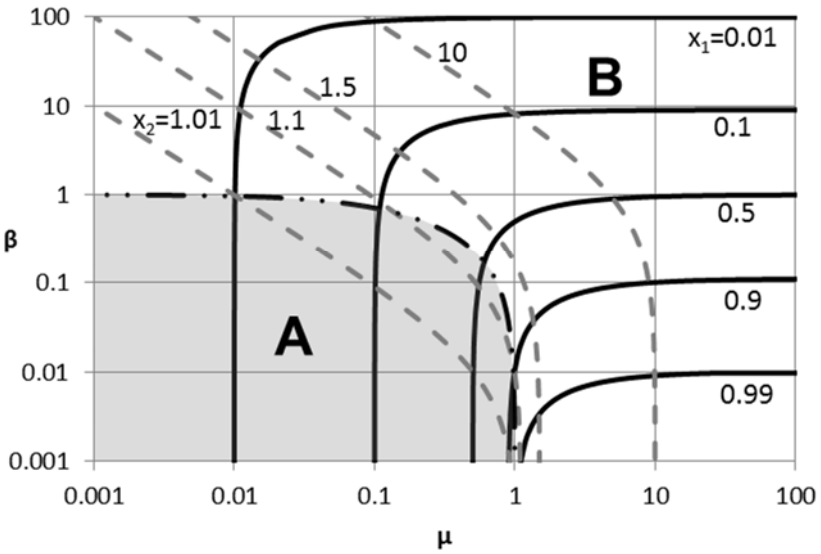

Figure 11: Variation of the mass ratio, β, as a function of the tuning parameter, μ, for different constant values of the dimensionless eigenvalues indicated in each curve. First eigenvalue x_1, solid lines; second eigenvalue x_2, dashed lines. Zone A corresponds for $m_{eff,1} < m_{eff,2}$; zone B corresponds for $m_{eff,1} > m_{eff,2}$. Dot-dashed line: $\mu_{0.5}$ according to Eq. (37).

For $\beta > 1$, the eigenvalues are placed in zone B, which implies that the first mode is the dominant ($m_{eff,1} > m_{eff,2}$), independently of the value of μ. The first mode is also dominant for $\mu > 1$, independently of the value of β. For $\beta << 1$, the boundary between zone A and zone B is close to $\mu = 1$.

3 Design cases

The design cases considered are focused on the determination of the values of the parameters that optimize the design of the structure according to the established requirements.

The requirement usually applied in the space industry that mostly influences the modal behavior of a satellite consists in establishing a minimum limit value for the main natural frequencies of the satellite f_{min} [2]. The minimum frequency specified in the requirement must be sufficiently larger than the maximum frequency of the excitation to reduce the risk of structural damage. This requirement affects the main modes of the system, which contribute most to the maximum forces and stresses generated by vibrations transmitted through the interface of the system. If the frequency of the excitation load coincides with one of the main natural frequencies, the effect of resonance increases the generated stresses that can lead to structural damage. The main modes of the system (e.g. the entire satellite) are defined as those modes whose modal effective mass fractions are above an established threshold $m_{eff,lim}$. For example, a typical value is 10% or 0.1 [2].

In this study, the minimum frequency requirement is only applied for modes whose modal effective mass fraction is above the established threshold. The modes with a modal effective mass fraction below the threshold are considered as local modes, whose contribution to the global response of the system is lower. These modes are related to the motion of small parts of the system and its excitation is less critical for the whole system than the excitation of modes with high modal effective mass, but it can be too severe for the affected small part. The

objective of the design cases proposed in this study is to know the limits of the values of the design parameters to assure that the whole system fulfills the imposed requirement, to finally obtain the optimum values of the design parameters within these limits.

Two different design cases are studied. The first design case refers to a design phase with the primary structure already determined (M and K known), while the secondary element is yet to be designed. The second design case is applied when the total mass is fixed but its distribution between the primary and secondary elements is yet to be decided.

To define the requirement of minimum natural frequency of the system in the first design case, the ratio between f_{min} and the reference frequency f_r is a fixed parameter. The values of the parameters of the main structure M and K are pre-established to achieve a reference natural frequency higher than f_{min}.

In the second case, the fixed parameter is the ratio between f_{min} and first natural frequency of the system when k is infinite, f_{10}. This case considers that the total mass, $M + m$, together with the main stiffness K, which directly define the value of f_{10}, are the pre-established parameters.

From the analytical point of view, the main difference between both design cases is that in the first case, the mass ratio β affects only the mass of the secondary part m, while in the second design case, the mass ratio β affects both the primary and the secondary masses. In this second design case, β indicates how the fixed total mass is divided between the primary and the secondary masses.

For both cases, the calculation of the range of values for the mass ratio β and the tuning parameter μ that allow the system to fulfill the specified requirement is determined according to the definition of the requirements, which differ in each design case. The analytical equations are obtained from the mathematical model explained in section 2. Finally, the optimum values of the design parameters are expressed in analytical form and are finally applied to the real case of the structural design of the UPMSat-2 satellite in section 4.

3.1 Design case 1: f_{min}/f_r as fixed parameter

In the first design case, the parameters related to the main structure are known and have been determined to get a reference natural frequency f_r sufficiently higher than the minimum natural frequency specified to the system,

$$f_r > f_{min}; \quad x_{min} = \left(\frac{f_{min}}{f_r} \right)^2 < 1 \tag{39}$$

As mentioned in section 2, the dynamic behavior of the system is altered by the addition of a small part of mass m with the generation of two modes, where the first mode is always lower than the reference mode.

The design region where the system does not fulfill the specified requirement corresponds to the shaded areas in Fig. 12 and it is defined by the intersection of the regions generated for each of the following inequalities

$$m_{eff,1} > m_{eff,lim} \tag{40a}$$

$$x_1 < x_{min} \tag{40b}$$

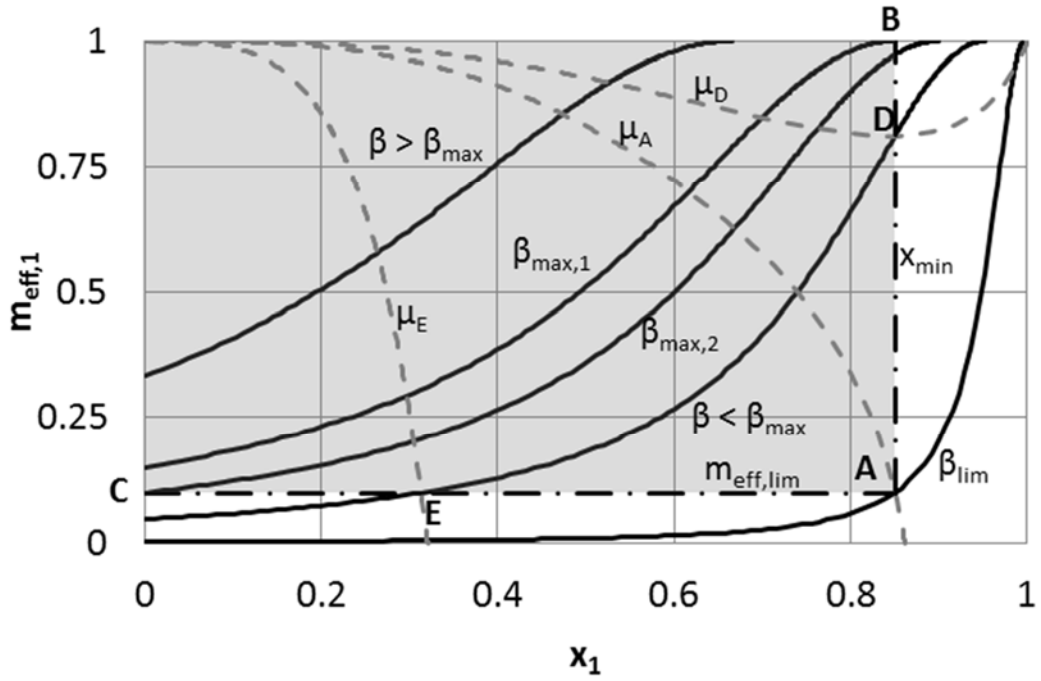

(a)

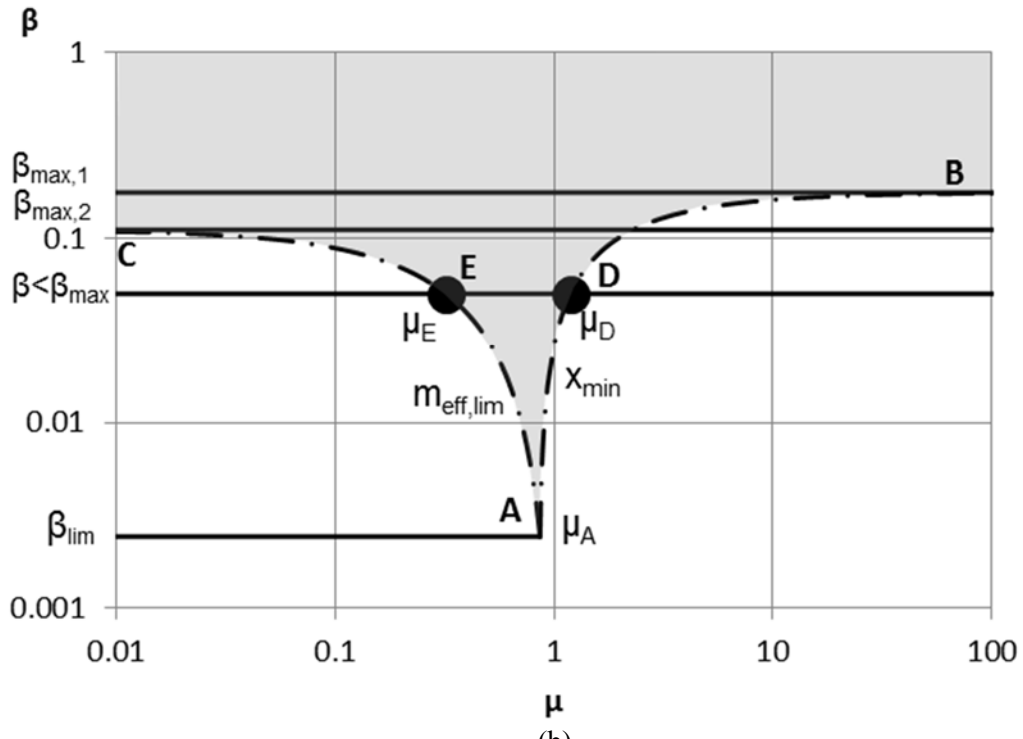

(b)

Figure 12: Example of design region (non-shaded area) for the first case according to the specified minimum natural frequency (x_{min} = 0.85, ADB limit) and modal effective mass fraction threshold ($m_{eff,lim}$ = 0.1, AEC limit). (a) Design region in $m_{eff,1} - x_1$ plane. (b) Design region in $\beta - \mu$ plane.

As shown in Fig. 12(b), there is a value for the mass ratio β_{max} above which the system will never fulfill the requirements. As shown in Fig. 12(a), the curve associated to a value of $\beta > \beta_{max}$ is entirely in the shaded area. This limit is the maximum between the limits $\beta_{max,1}$ and $\beta_{max,2}$. $\beta_{max,1}$ is related to the established minimum eigenvalue x_{min} (AB), and $\beta_{max,2}$ is related to the modal effective mass fraction threshold $m_{eff,lim}$ (AC).

The first limit $\beta_{max,1}$ is calculated considering the maximum value for the first dimensionless eigenvalue for a 2-DOF system, x_{10}, which is the case when both the stiffness between the two masses, k, and the tuning parameter μ are infinite. This parameter is defined as

$$x_{10} \equiv \left(\frac{\omega_{10}}{\omega_r} \right)^2 = \frac{K \big/ (M+m)}{K \big/ M} = \frac{M}{M+m} = \frac{1}{1+\beta} \tag{41}$$

This value of x_{10} constitutes the upper limit for the lowest dimensionless eigenvalue x_1 for a given value of the mass ratio β. The maximum mass ratio $\beta_{max,1}$ that can provide a first eigenvalue of the 2-DOF system above x_{min} is calculated using Eq. (41) for $x_{10} = x_{min}$

$$\beta_{max,1} = \frac{1 - x_{min}}{x_{min}} \tag{42}$$

This value is the asymptotic limit of the design region for $\mu \to \infty$ indicated in Fig. 12(b) and that corresponds to point B in Fig. 12(a).

The value of $\beta_{max,2}$ is the maximum value of mass ratio that can provide a modal effective mass fraction below or equal to the threshold of $m_{eff,lim}$. For a given mass ratio β, the minimum value of modal effective mass fraction of the first mode for a 2-DOF system is obtained from Eq. (33a) for $\mu = 0$

$$m_{eff,1} = \frac{\beta}{1+\beta} \tag{43}$$

For $m_{eff,1} = m_{eff,lim}$, the value of $\beta_{max,2}$ is

$$\beta_{max,2} = \frac{m_{eff,lim}}{1 - m_{eff,lim}} \tag{44}$$

This value is the limit of the design region for $\mu \to 0$, which corresponds to the point C in Fig. 12(a).

Therefore, the maximum value of the mass ratio β_{max} for which the system can meet the requirement is

$$\beta_{max} = \max\left(\frac{1-x_{min}}{x_{min}}, \frac{m_{eff,lim}}{1-m_{eff,lim}} \right) \tag{45}$$

For values of mass ratio β above this maximum value β_{max}, the 2-DOF system will never exhibit a first natural frequency higher than f_{min}. Also, the modal effective mass fraction for the first mode is higher than $m_{eff,lim}$.

There is a value for the mass ratio β_{lim} below which the system always meets the requirement, independently of the value of μ. This configuration is identified as the point A in Fig. 12. The value of β_{lim} is calculated with Eq. (25) for $x_1 = x_{min}$ and $m_{eff,1} = m_{eff,lim}$

$$\beta_{lim}{}^2 + \beta_{lim}\left[1 + \left(\frac{1-x_{min}}{x_{min}} \right)^2 - \frac{1}{m_{eff,lim}} \left(1 + \frac{1-x_{min}}{x_{min}} \right)^2 \right] + \left(\frac{1-x_{min}}{x_{min}} \right)^2 = 0 \tag{46}$$

Defining $x'_{min} \equiv \dfrac{1-x_{min}}{x_{min}}$

the result is

$$\beta_{lim} = \frac{1}{2}\left[\frac{1}{m_{eff,lim}}\left(1+x'_{min}\right)^2 - 1 - x'_{min}{}^2 - \sqrt{\left[\frac{1}{m_{eff,lim}}\left(1+x'_{min}\right)^2 - 1 - x'_{min}{}^2 \right]^2 - 4x'_{min}{}^2} \right] \tag{47}$$

The value of the tuning parameter in this point is defined as μ_A, and can be calculated using Eq. (30) for $\beta = \beta_{lim}$ and $m_{eff,i} = m_{eff,lim}$.

For the case where the mass ratio β are between β_{max} and β_{lim}, there is a range of values for the tuning parameter μ within which the system does not fulfill the requirements. This range corresponds to the segment between points E and D in Fig. 12. For values higher than the upper limit of this range μ_D, the first natural frequency of the system is above the minimum frequency established in the requirement. For values of the tuning parameter below the lower limit of this range, μ_E, the modal effective mass fraction of the first mode is below the threshold established, and therefore is allowed to have a natural frequency below the required minimum value.

The expression of μ_D for a given mass ratio β between β_{lim} and $\beta_{max,1}$ is calculated from Eq. (15) for $x_1 = x_{min}$

$$\mu_D = \frac{1-x_{min}}{\dfrac{1-x_{min}}{x_{min}} - \beta} \tag{48}$$

This value corresponds to the point D in Fig. 12.

The lower limit μ_E of the range is identified with the point E in Fig. 12. This value is calculated from Eq. (30) for β between β_{lim} and $\beta_{max,2}$ and for $m_{eff,1} = m_{eff,lim}$

$$\mu_E = \frac{\left(1-\sqrt{\beta\frac{1-m_{eff,lim}}{m_{eff,lim}}}\right)\left(\beta+\sqrt{\beta\frac{1-m_{eff,lim}}{m_{eff,lim}}}\right)}{\sqrt{\beta\frac{1-m_{eff,lim}}{m_{eff,lim}}}\left(1+\beta\right)^2} \tag{49}$$

For designs where $\mu > \mu_D$, the lowest natural frequency of the system is $f_1 > f_{min}$ and therefore, the system meets the requirement. In this situation, this first mode is considered as main mode of the system because its modal effective mass fraction is higher than the threshold $m_{eff,lim}$.

For the case where $\mu < \mu_E$, the lowest mode of the system can be considered as a local mode because it has a modal effective mass fraction below the established threshold. From the whole system point of view, this design region is allowed, even though the first natural frequency is below f_{min}, because the excitation of this mode has less influence on the global response of the system. But there is a considerable risk of damage for the small part, which must be taken into account.

After establishing the limits of the design region, the optimum design is defined as the point of this region that minimizes the structural mass, which is directly influenced by the stiffness. In this design case, the variable parameters are related to the secondary mass. In many situations, the main contribution of the total mass of a system like a satellite or a payload is due to the non-structural elements. For this reason, in the optimization example exposed below, the small mass m and the mass ratio β are fixed values independent of the structural parameters as the stiffness k and the tuning parameter μ. The objective is the calculation of the minimum values of the stiffness k and the natural frequency f_{20} of the small part for given values of M, K, m and β.

For the design region where $\mu < \mu_E$, the theoretical optimum design is obtained for $\mu \to 0$. In this design region, the drawback is the risk of damage to the small part due to the amplification at the resonance of the local mode with the low frequency excitations. For this reason, the considered design region in this optimization is for $\mu > \mu_D$, where the natural frequencies of the system are higher than f_{min}. For a value of the mass ratio between β_{lim} and $\beta_{max,1}$, the optimum design point is when the structural mass and thus the stiffness k of the secondary part is minimum. The minimum stiffness within the design region limits is for $\mu = \mu_D$. From Eq. (48), the following expression is obtained

$$\frac{\mu_D}{x_{min}} = \frac{1}{1-\frac{x_{min}}{1-x_{min}}\beta} \tag{50}$$

Expressed in terms of natural frequencies is

$$f_{20,opt} = f_{min} \sqrt{\frac{1}{1 - \frac{f_{min}^{\ 2}}{f_r^{\ 2} - f_{min}^{\ 2}} \beta}} \tag{51}$$

The optimum stiffness of the small part is

$$k_{opt} = 4\pi^2 m f_{min}^{\ 2} \frac{1}{1 - \frac{f_{min}^{\ 2}}{f_r^{\ 2} - f_{min}^{\ 2}} \beta} \tag{52}$$

And the optimum stiffness ratio α_{opt} is

$$\alpha_{opt} = \mu_D \beta = \frac{\beta x_{min}}{1 - \frac{x_{min}}{1 - x_{min}} \beta} = \frac{x_{min}}{\frac{1}{\beta} - \frac{x_{min}}{1 - x_{min}}} \tag{53}$$

Eq. (51) is a useful expression that can be employed to derive a specification for the minimum natural frequency to a secondary part, $f_{20,opt}$, with the aim to avoid that the first frequency of the whole system is below a specified f_{min}.

3.2 Design case 2: f_{10}/f_r as fixed parameter

With the same purpose as in the previous case, a minimum limit is established for the main natural frequencies of the system. Like in the first design case, this requirement only affects the main modes of the system, i.e. those with a modal effective mass fraction above an established threshold. The difference in this case is that the known or fixed parameters are the total mass of the system, $M + m$, and the primary stiffness K. With both parameters, the maximum first natural frequency of the 2-DOF system can be calculated considering that the stiffness k between the two masses is infinite

$$f_{10} = \frac{1}{2\pi} \sqrt{\frac{K}{M + m}} \tag{54}$$

$$x_{10} = \left(\frac{f_{10}}{f_r} \right)^2 = \frac{K / (M + m)}{K / M} = \frac{1}{1 + \beta} \tag{55}$$

In this second case, the parameter φ is defined as the ratio between f_{min} and f_{10}. The requirement is expressed as follows

$$\varphi \equiv \frac{f_{min}}{f_{10}} < 1 \tag{56}$$

The risk region is defined by the intersection of the regions generated for each of these inequalities

$$m_{eff,1} > m_{eff,lim} \tag{57a}$$

$$f_1 < f_{min}; \quad \left(\frac{f_1}{f_{10}}\right)^2 = \frac{x_1}{x_{10}} < \left(\frac{f_{min}}{f_{10}}\right)^2 = \varphi^2; \quad x_1 < x_{10}\varphi^2 \tag{57b}$$

Using Eq. (55), the expression for the minimum limit for the dimensionless eigenvalue is given by

$$x_{min} = \frac{\varphi^2}{1+\beta} \tag{58}$$

In this second design case, x_{min} depends on the mass ratio β unlike in the first design case, where x_{min} is a constant value. The design region corresponds to the non-shaded areas in Fig. 13.

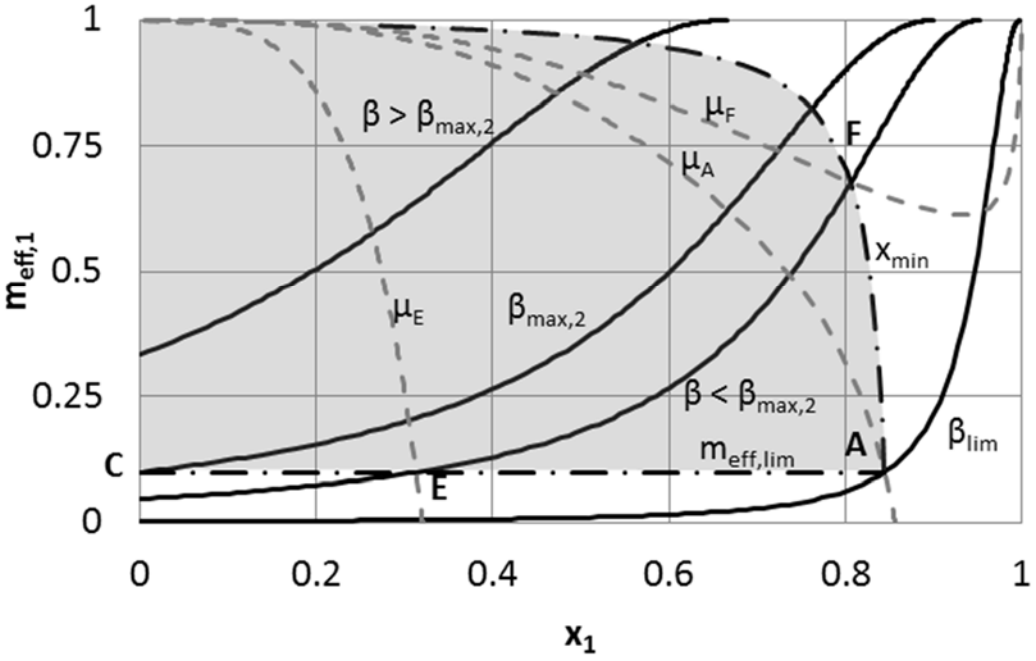

(a)

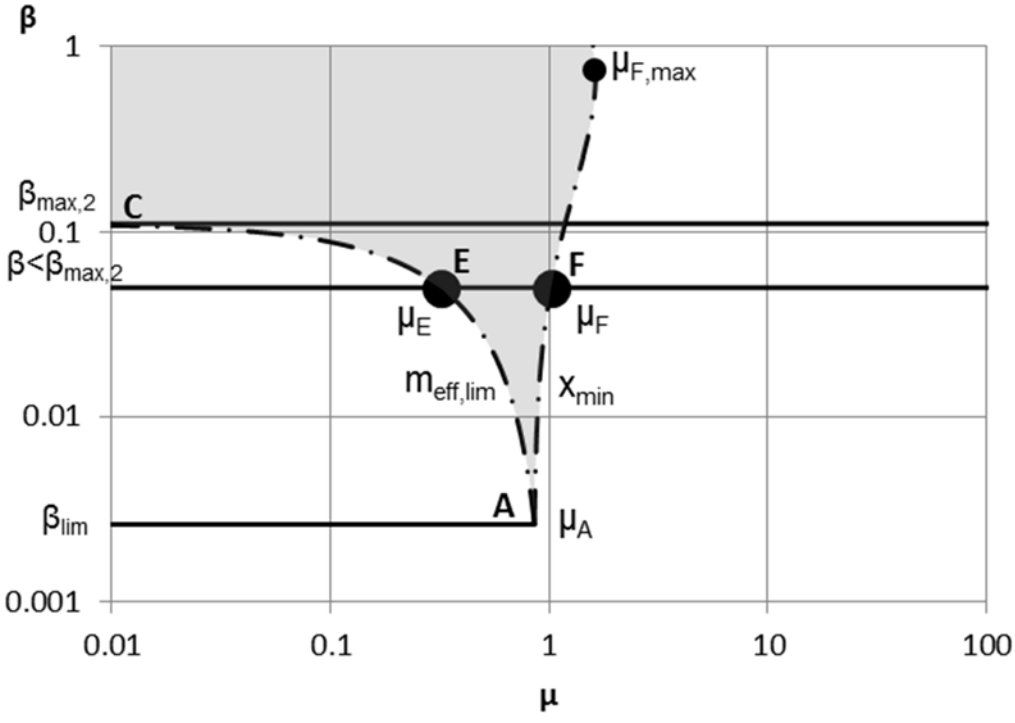

(b)

Figure 13: Example of design region (non-shaded area) for the second case according to the specified minimum natural frequency (φ = 0.92, AF limit) and modal effective mass fraction threshold ($m_{eff,lim}$ = 0.1, AEC limit). (a) Design region in $m_{eff,1} - x_1$ plane. (b) Design region in $\beta - \mu$ plane.

The equations that relate the modal effective mass fraction $m_{eff,1}$ with the frequency ratio φ and the minimum dimensionless eigenvalue x_{min} are obtained from Eqs. (25), (26) and (58)

$$m_{eff,1} = \frac{1}{1 + \frac{x_{min}}{\varphi^2 - x_{min}}\left(1-\varphi^2\right)^2} \tag{59}$$

$$x_{min} = \frac{\varphi^2}{1 + \frac{m_{eff,1}}{1-m_{eff,1}}\left(1-\varphi^2\right)^2} \tag{60}$$

The curve AF that sets the upper limit of the shaded area in Fig. 13(a) is given by Eq. (60).

The value of $\beta_{max,2}$ has the same meaning and expression as in the first design case. The difference in this second case is that the maximum value of the mass ratio β_{max} above which the 2-DOF system cannot fulfill the requirement does not exist, i.e. it is possible to fulfill the requirement for any value of β, depending on the value of the tuning parameter μ.

As in the first design case, there is a value for the mass ratio β_{lim} below which the 2-DOF system always complies with the requirement, independently of the value of μ. This value is represented in Fig. 13 as the point A, and is calculated using Eq. (25) and Eq. (56) for x_1 for x_{min}, $m_{eff,1}$ for $m_{eff,lim}$ and $\beta = \beta_{lim}$

$$m_{eff,lim} = \frac{\beta_{lim}}{1+\beta_{lim}} \frac{\left[1 + \left(\frac{1-x_{min}}{x_{min}}\right)\right]^2}{\left[\beta_{lim} + \left(\frac{1-x_{min}}{x_{min}}\right)^2\right]} = \frac{\beta_{lim}}{1+\beta_{lim}} \frac{\frac{\left(1+\beta_{lim}\right)^2}{\varphi^4}}{\left(1+\beta_{lim}\right)\frac{\beta_{lim}+\left(1-\varphi^2\right)^2}{\varphi^4}} = \frac{\beta_{lim}}{\beta_{lim}+\left(1-\varphi^2\right)^2}$$

$$\beta_{lim} = \frac{m_{eff,lim}}{1-m_{eff,lim}}\left(1-\varphi^2\right)^2 \tag{61}$$

The value of μ_A in this point is obtained using Eq. (15), for $\beta = \beta_{lim}$ and $x_i = x_{min}$

$$\mu_A = \frac{1-x_{min}}{\frac{1-x_{min}}{x_{min}} - \beta_{lim}} = \frac{1}{\frac{1}{x_{min}} - \frac{\beta_{lim}}{1-x_{min}}} = \frac{1}{\frac{1+\beta_{lim}}{\varphi^2} - \frac{\beta_{lim}\left(1+\beta_{lim}\right)}{1+\beta_{lim}-\varphi^2}} \tag{62}$$

$$\mu_A = \frac{\varphi^2\left(1+\beta_{lim}-\varphi^2\right)}{\left(1+\beta_{lim}\right)^2\left(1-\varphi^2\right)} = \frac{\varphi^2\left(1-m_{eff,lim}\right)\left(1-\varphi^2\left(1+m_{eff,lim}\right)+\varphi^4 m_{eff,lim}\right)}{\left(1-\varphi^2\right)\left(1-2\varphi^2 m_{eff,lim}+\varphi^4 m_{eff,lim}\right)^2} \tag{63}$$

For values of $\beta > \beta_{lim}$, there is a minimum value for the tuning parameter, μ_F, above which the system has a first natural frequency above f_{min}. This design point is indicated as point F in Fig. 13 for a given mass ratio β. The value of μ_F is obtained from Eq. (15) and with the same procedure shown in Eqs. (62) and (63)

$$\mu_F = \frac{\varphi^2\left(1+\beta-\varphi^2\right)}{\left(1+\beta\right)^2\left(1-\varphi^2\right)} \tag{64}$$

As can be seen in Fig. 13(b), there is a value of the mass ratio β that maximizes the value for μ_F (curve AF). This means that for $\mu > \mu_{F,max}$, the first natural frequency is higher than the specified minimum frequency f_{min} for the whole range of values of β. This maximum value, $\mu_{F,max}$, is obtained by deriving the expression in Eq. (64)

$$\frac{\partial \mu_F}{\partial \beta} = 0; \quad \beta = -1 + 2\varphi^2 \tag{65}$$

and substituting in Eq. (64)

$$\mu_{F,max} = \frac{1}{4\left(1-\varphi^2\right)} \tag{66}$$

The expression of the maximum value $\mu_{F,max}$ in Eq. (66) is only applicable for $\varphi^2 \geq 0.5$. A design with the mass ratio β given by Eq. (65) can fulfill the requirement if $\mu > \mu_{F,max}$, even being higher than $\beta_{max,2}$, because in this situation the first mode has a natural frequency above the imposed minimum value and with a modal effective mass fraction above the established threshold.

For $\varphi^2 < 0.5$, the maximum value $\mu_{F,max}$ is for $\beta = 0$ and, using Eq. (64), is given by

$$\mu_{F,max} = \varphi^2 \tag{67}$$

Like in the first design case, for the range of values of the mass ratio between β_{lim} (point A) and $\beta_{max,2}$ (point C), there is a limit μ_E that is defined when the modal effective mass fraction of the first mode is equal to the threshold indicated in the specification. The expression obtained for the first design case to calculate this limit (Eq. (49)) is also valid for this second design case. For $\mu < \mu_E$, the first natural frequency of the system is lower than the specified minimum value f_{min}, but with an associated modal effective mass fraction below the threshold established to identify the main modes of the system.

The optimum design that gets a first natural frequency of the system above the specified minimum value f_{min} is when $\mu = \mu_F$. The optimum stiffness ratio using Eq. (64) is

$$\alpha_{opt} = \mu_F \beta = \frac{\varphi^2 \beta \left(1+\beta-\varphi^2\right)}{\left(1+\beta\right)^2 \left(1-\varphi^2\right)} \tag{68}$$

The optimum stiffness k_{opt} of the small part can be calculated by using Eqs. (68) and (55)

$$k_{opt} = \alpha_{opt} K = \frac{\varphi^2 \beta \left(1+\beta-\varphi^2\right)}{\left(1+\beta\right)^2 \left(1-\varphi^2\right)} K$$

$$k_{opt} = \frac{\varphi^2 \beta \left(1+\beta-\varphi^2\right)}{\left(1+\beta\right)^2\left(1-\varphi^2\right)}\left(2\pi f_{10}\right)^2\left(M+m\right) = 4\pi^2 m {f_{min}}^2 \frac{\left(1+\beta-\varphi^2\right)}{\left(1+\beta\right)\left(1-\varphi^2\right)} \tag{69}$$

The minimum natural frequency of the small part when its interface is constrained is given by

$$f_{20,opt} = \frac{1}{2\pi}\sqrt{\frac{k_{opt}}{m}} = f_{\min}\sqrt{\frac{\left(1+\beta-\varphi^2\right)}{\left(1+\beta\right)\left(1-\varphi^2\right)}} \tag{70}$$

Defining $\beta^* \equiv \dfrac{m}{M+m} = \dfrac{\beta}{1+\beta}$

$$f_{20,opt} = f_{min}\sqrt{1+\beta^*\frac{\varphi^2}{1-\varphi^2}} = f_{min}\sqrt{1+\beta^*\frac{{f_{min}}^2}{{f_{10}}^2-{f_{min}}^2}} \tag{71}$$

Eq. (71) can be used by the satellite designers to derive a specification of minimum natural frequency to be imposed as a requirement for its subsystems to assure that the first natural frequency of the entire satellite is above the minimum value f_{min} defined by the launch authority. The input parameters for this equation are f_{min}, the mass ratio of the subsystem or instrument with respect to the total mass β^* and the first natural frequency f_{10} of the satellite considering the subsystem as a rigid body attached to the main structure. Using Eq. (71), the value of $f_{20,opt}$ increases when the mass ratio β^* increases, indicating that the requirement is more severe for massive subsystems.

An example of the design of a lateral panel of the microsatellite UPMSat-2 is explained in section 4, where the expressions presented in this study are used to compare with the results of the finite element model (FEM).

4 Case study: design of lateral panels of the UPMSat-2 university class microsatellite

UPMSat-2 is a microsatellite developed by the Spanish university research institute Instituto Universitario de Microgravedad "Ignacio Da Riva" (IDR) of the Universidad Politécnica de Madrid (UPM), Spain [37, 38]. The structure, shown in Fig. 14(a), presents a prismatic shape composed by four squared stiffened trays, located horizontally at different heights, and attached to four vertical beams at each corner. The lateral faces of the satellite are composed of four vertical double panels, where the solar cells of the satellite and the corresponding harnesses are distributed on the exterior side of the outer panels.

A study about the structural design of the lateral panels shown in Fig. 14(b) is carried out to evaluate the effect of the local modes of these parts on the global modes of the satellite. In this study, two equal opposite panels are considered as the secondary part. The simplified model that best represents this configuration consists of two small masses connected in parallel to the large mass that represents the rest of the satellite. But taking into account that both panels are identical in mass and stiffness, the results are the same when considering the 2-DOF

mathematical model developed in section 2, where the small mass m is the sum of the masses of both panels including their non-structural mass distributions, and the small stiffness k is also the sum of the equivalent stiffness of each panel.

In the designs analyzed in this work, the considered mechanical interface between each outer panel with the rest of the satellite structure consists of a distribution of bolts along the two vertical edges that attach it to the vertical beams of the satellite. The natural frequency of the isolated secondary part (f_{20}) can be calculated by the FEM of one outer panel by constraining the interface nodes of the 1D CBUSH elements that represent the bolts.

The large mass M corresponds to the rest of the satellite with a value of 41.88 kg. The reference natural frequency f_r = 54.02 Hz is the first lateral mode of the satellite without the considered two outer panels, which has been calculated from FEM analysis (Fig. 15(a)). The objective is to determine, for different design options of the outer panels, if the satellite can fulfill the requirement of having lateral modes above 45 Hz, which is the value specified for the microsatellites that are attached to the secondary payloads adapter of the Ariane 5 launch vehicle [39].

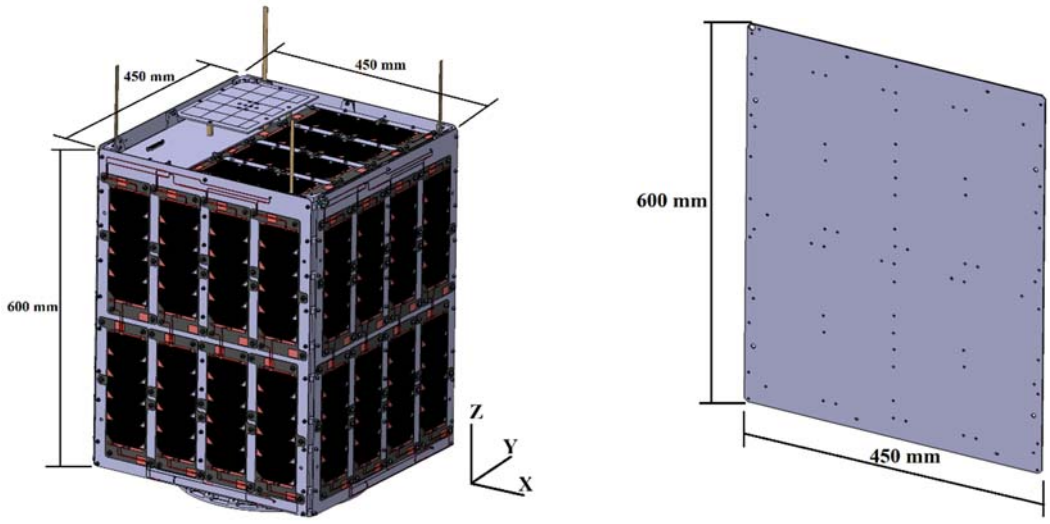

(a) UPMSat-2 design. b) Outer lateral panels.

Figure 14: UPMSat-2 and a lateral panel without solar cells.

In the first design option of the outer panels (case 1), the mass of the two outer panels with their non-structural elements is m = 4.92 kg. The mass ratio between the large and the small masses is β = 0.118, and the first mode of the constrained panel obtained from FEM analysis is f_{20}^{FEM} = 48.99 Hz (Fig. 15(b)). The maximum first global mode of the satellite for the case where the panels are infinitely rigid is f_{10} = 51.10 Hz, which has been estimated using Eq. (55) from the given mass ratio β and reference frequency f_r.

The parameters and the results are shown in Table 1, comparing the prediction of the first global mode of the entire satellite with the 2-DOF mathematical approach (f_1 = 43.42 Hz) and the result obtained by FEM analysis (f_1^{FEM} = 43.55 Hz), where the modal shape is shown in Fig. 15(c). The difference between both calculations is below 1%. With this design, the lateral frequency of the satellite is below the specified minimum frequency and it is necessary to improve the design by increasing the stiffness of the panels to fulfill the requirement. With this objective, Eq. (71) is used to analytically estimate the minimum frequency of the isolated panels

considering negligible the increase of their structural mass. The result is that this mode must be at least $f_{20,opt}$ = 52.54 Hz.

A second case with a slight modification of the stiffness in the FEM of the panels to reach this optimum frequency provides a mode of f_{20}^{FEM} = 52.97 Hz for the constrained panel, and a first global mode of the satellite of f_1^{FEM} = 45.01 Hz. The requirement is fulfilled in this second case.

To have a more conservative design, a third case is proposed with a greater increase in the stiffness of the panels, which implies a non-negligible increase of the structural mass. In this case, the total mass of both outer panels reaches 5.35 kg (β = 0.128) and the local mode is f_{20}^{FEM} = 64.79 Hz. The global mode obtained from FEM analysis is f_1^{FEM} = 47.01 Hz, while the analytical prediction gives a value of f_1 = 47.76 Hz.

The difference of frequencies between analytical predictions and FEM results increases for the cases studied as the modal effective mass fraction of the fundamental mode of the constrained panel decreases as consequence of the modification the design. Therefore, assuming this panel as a single degree of freedom system becomes less consistent due to a higher contribution of the rest of the modes of the panel. Nevertheless, the differences of frequencies between analytical predictions and FEM results are below 2% in all studied cases.

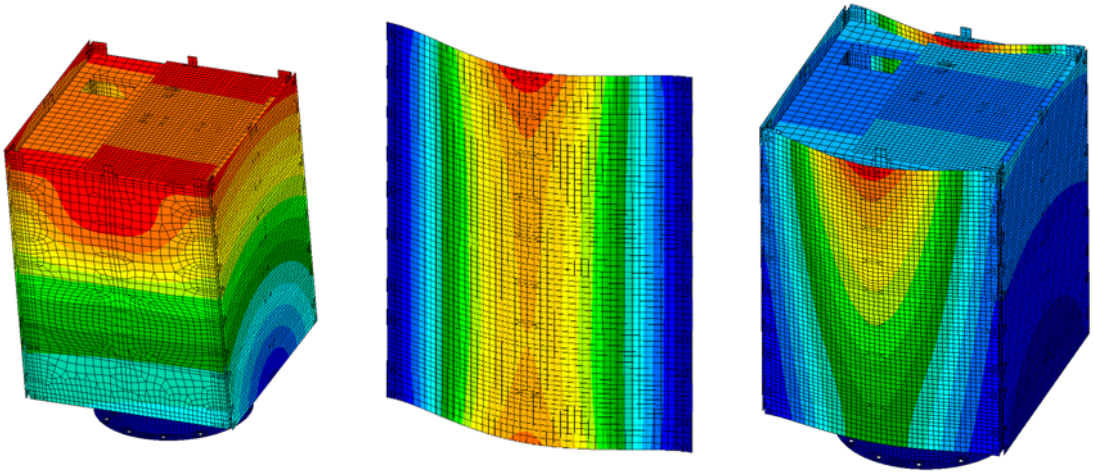

(a) Reference global mode of the satellite without outer panels (f_r = 54.02 Hz).

(b) Local mode of the isolated outer lateral panel in Case 1 (f_{20}^{FEM} = 48.99 Hz).

(c) First lateral mode of the entire model in Case 1 (f_1^{FEM} = 43.55 Hz).

Figure 15: Finite Element Model Results of UPMSat-2.

Table 1: Results of three design cases for the lateral panels of UPMSat-2.

Parameters	Case 1	Case 2	Case 3
β	0.118	0.118	0.128
f_r (Hz)	54.02	54.02	54.02
x_{min}	0.694	0.694	0.694
f_{20}^{FEM} (Hz)	48.99	52.97	64.79
μ	0.822	0.961	1.438
x_1 (2-DOF approach)	0.646	0.699	0.781
f_1 (Hz) (2-DOF approach)	43.42	45.17	47.76
f_1^{FEM} (Hz)	43.55	45.01	47.01
Relative difference	-0.30%	0.34%	1.58%

5 Conclusions

This study presents an analytical approach to describe the effects of the dynamic coupling between a secondary and a primary structure (in terms of their mass ratio and tuning parameter) on the modification of natural frequencies, mode shapes and modal effective masses of the whole structure. This case appears in several designs of space structures, for example for instruments or components that have natural frequencies close to the natural frequencies of the spacecraft. The dynamic coupling has been evaluated with an undamped 2-DOF mathematical model presented and solved in section 2. Considering this undamped model has allowed to obtain useful analytical expressions with the advantage of providing a rapid and direct estimation of the influence of design parameters, as mass ratio β and tuning parameter μ, on the main results. These results allow to carry out studies on the preliminary design phase of spacecraft by means of these values and feasible and unfeasible design regions. This method has been compared with other alternatives such as Dunkerley's and Rayleigh's methods to calculate the first natural frequency of the system, showing that the proposed method has the advantage of providing exact solutions for all range of values of the design parameters and with ease-of-use expressions. This study has demonstrated how the main mode of the system can be appreciably altered when the local mode of the small part has a similar frequency, even for negligible values of the mass of the small part. The effect is the division of the global mode into two modes, where both modes can have similar values of modal effective mass fraction. Another important consequence is the decrease of the first natural frequency of the satellite, which can lead to the unfulfillment of the requirement of minimum natural frequency imposed by the launcher to prevent the structural resonance with the loads generated during the launch phase. Therefore, the mathematical equations presented in this work provide an easy way of calculation to find out the optimum values for a preliminary design of a secondary part for the case where the modal coupling of this part with the entire satellite cannot be avoided. The objective is to find the design values so that the satellite can fulfill the minimum natural frequency requirement. These equations can be useful to the satellite designers to derive a specification of minimum natural frequency to be imposed on the payloads. The analytical approach presented in this work has been applied to the design of the structural lateral panels of the microsatellite UPMSat-2, where the differences with respect to FEM calculations are below 2%.

Acknowledgements

This work has been partially funded by the Spanish "Ministerio de Economía, Industria y Competitividad" through project ESP2015-65064-C2-2-P.

References

[1] J.J. Wijker, Spacecraft Structures, Springer Berlin Heidelberg, Berlin, Heidelberg, 2008. doi:10.1007/978-3-540-75553-1.

[2] ECSS, ECSS-E-HB-32-26A, Space engineering, Spacecraft mechanical loads analysis handbook, ESA-ESTEC Requirements and Standards Division, Noordwijk, The Netherlands, 2013.

[3] A. Bertram, Dynamic qualification of large space structures by means of modal coupling techniques, Acta Astronaut. 7 (1980) 1179–1190. doi:10.1016/0094-5765(80)90070-3.

[4] A.K. Gupta, J.-W. Jaw, Coupled response spectrum analysis of secondary systems using uncoupled modal properties, Nucl. Eng. Des. 92 (1986) 61–68. doi:10.1016/0029-5493(86)90099-3.

[5] J.H. Lim, A correlation study of satellite finite element model for coupled load analysis using transmissibility with modified correlation measures, Aerosp. Sci. Technol. 33 (2014) 82–91. doi:10.1016/j.ast.2014.01.002.

[6] J.H. Lim, D.S. Hwang, K.W. Kim, G.H. Lee, J.G. Kim, A coupled dynamic loads analysis of satellites with an enhanced Craig–Bampton approach, Aerosp. Sci. Technol. 69 (2017) 114–122. doi:10.1016/j.ast.2017.06.023.

[7] J.F. Mercer, G.S. Aglietti, M. Remedia, A. Kiley, An assessment of spacecraft target mode selection methods, Acta Astronaut. 140 (2017) 537–553. doi:10.1016/j.actaastro.2017.09.013.

[8] Y.Q. Tu, G.T. Zheng, On the Vibration Isolation of Flexible Structures, J. Appl. Mech. 74 (2007) 415. doi:10.1115/1.2201882.

[9] Y. Chen, B. Fang, T. Yang, W. Huang, Study of Whole-spacecraft Vibration Isolators Based on Reliability Method, Chinese J. Aeronaut. 22 (2009) 153–159. doi:10.1016/S1000-9361(08)60081-3.

[10] L. Liu, J. Shan, Y. Zhang, Dynamics Modeling and Analysis of Spacecraft with Large Deployable Hoop-Truss Antenna, J. Spacecr. Rockets. 53 (2016) 471–479. doi:10.2514/1.A33464.

[11] S. Waimer, S. Manzato, B. Peeters, M. Wagner, P. Guillaume, Special Topics in Structural Dynamics, Volume 6, Springer International Publishing, Cham, 2017. doi:10.1007/978-3-319-53841-9.

[12] H. Frahm, Device for damping vibrations of bodies, 989958, 1911.

[13] J.P. Den Hartog, Mechanical Vibrations, Third Edit, McGraw-Hill Book Company, Inc, New York and London, 1947.

[14] R. Rana, T.T. Soong, Parametric study and simplified design of tuned mass dampers, Eng. Struct. 20 (1998) 193–204. doi:http://dx.doi.org/10.1016/S0141-0296(97)00078-3.

[15] T. Taniguchi, A. Der Kiureghian, M. Melkumyan, Effect of tuned mass damper on displacement demand of base-isolated structures, Eng. Struct. 30 (2008) 3478–3488. doi:10.1016/j.engstruct.2008.05.027.

[16] A.A. Farghaly, M. Salem Ahmed, Optimum Design of TMD System for Tall Buildings, ISRN Civ. Eng. 2012 (2012) 1–13. doi:10.5402/2012/716469.

[17] C.C. Lin, L.Y. Lu, G.L. Lin, T.W. Yang, Vibration control of seismic structures using semi-active friction multiple tuned mass dampers, Eng. Struct. 32 (2010) 3404–3417. doi:10.1016/j.engstruct.2010.07.014.

[18] F. Behnamfar, S. Dorafshan, A. Taheri, B. Hosseini Hashemi, A method for rapid estimation of dynamic coupling and spectral responses of connected adjacent structures, Struct. Des. Tall Spec. Build. 25 (2016) 605–625. doi:10.1002/tal.1274.

[19] V. Umachagi, K. Venkataramana, G.R. Reddy, R. Verma, Applications of Dampers for Vibration Control of Structures : an Overview, Int. J. Res. Eng. Technol. (2013) 6–11.

[20] K. Engelen, H. Ramon, W. Saeys, W. Franssens, J. Anthonis, Positioning and tuning of viscous damper on flexible structure, J. Sound Vib. 304 (2007) 845–862. doi:10.1016/j.jsv.2007.03.020.

[21] X.T.X. Tang, L.Z.L. Zuo, Regenerative semi-active control of tall building vibration with series TMDs, Am. Control Conf. (ACC), 2010. (2010) 5094–5099. doi:10.1109/ACC.2010.5530485.

[22] F. Weber, Optimal semi-active vibration absorber for harmonic excitation based on controlled semi-active damper, Smart Mater. Struct. 23 (2014). doi:10.1088/0964-1726/23/9/095033.

[23] G.L. Lin, C.C. Lin, B.C. Chen, T.T. Soong, Vibration control performance of tuned mass dampers with resettable variable stiffness, Eng. Struct. 83 (2015) 187–197. doi:10.1016/j.engstruct.2014.10.041.

[24] P. Brzeski, M. Lazarek, P. Perlikowski, Experimental study of the novel tuned mass damper with inerter which enables changes of inertance, J. Sound Vib. 404 (2017) 47–57. doi:10.1016/j.jsv.2017.05.034.

[25] S.K. Mishra, S. Gur, S. Chakraborty, An improved tuned mass damper (SMA-TMD) assisted by a shape memory alloy spring, Smart Mater. Struct. 22 (2013). doi:10.1088/0964-1726/22/9/095016.

[26] K.W. Min, J. Kim, Y.W. Kim, Design and test of tuned liquid mass dampers for attenuation of the wind responses of a full scale building, Smart Mater. Struct. 23 (2014). doi:10.1088/0964-1726/23/4/045020.

[27] M.J. Hochrainer, P.A. Fotiu, Design of coupled tuned liquid column gas dampers for multi-mode reduction in vibrating structures, Acta Mech. 229 (2018) 911–928. doi:10.1007/s00707-017-2007-0.

[28] F. Bourquin, G. Caruso, M. Peigney, D. Siegert, Magnetically tuned mass dampers for optimal vibration damping of large structures, Smart Mater. Struct. 23 (2014). doi:10.1088/0964-1726/23/8/085009.

[29] F. Weber, C. Boston, M. Maślanka, An adaptive tuned mass damper based on the emulation of positive and negative stiffness with an MR damper, Smart Mater. Struct. 20 (2011). doi:10.1088/0964-1726/20/1/015012.

[30] F. Weber, M. Maślanka, Frequency and damping adaptation of a TMD with controlled MR damper, Smart Mater. Struct. 21 (2012). doi:10.1088/0964-1726/21/5/055011.

[31] P. Bonello, S. Rafique, R. Shuttleworth, A theoretical study of a smart electromechanical tuned mass damper beam device, Smart Mater. Struct. 21 (2012). doi:10.1088/0964-1726/21/12/125004.

[32] B. Esser, D. Huston, Active mass damping of electronic circuit boards, J. Sound Vib. 277 (2004) 419–428. doi:10.1016/j.jsv.2003.11.055.

[33] Y.Q. Guo, W.Q. Chen, Dynamic analysis of space structures with multiple tuned mass dampers, Eng. Struct. 29 (2007) 3390–3403. doi:10.1016/j.engstruct.2007.09.004.

[34] A.J. Yingling, B.N. Agrawal, Applications of tuned mass dampers to improve performance of large space mirrors, Acta Astronaut. 94 (2014) 1–13. doi:10.1016/j.actaastro.2013.07.039.

[35] H. Garrido, O. Curadelli, D. Ambrosini, Semi-active friction tendons for vibration control of space structures, J. Sound Vib. 333 (2014) 5657–5679. doi:10.1016/j.jsv.2014.06.018.

[36] J.S. Hwang, H. Kim, Mode decomposition of structures with closely distributed modes and nonclassical damping, Struct. Control Heal. Monit. 25 (2018) 1–14. doi:10.1002/stc.2065.

[37] J. Cubas, A. Farrahi, S. Pindado, Magnetic Attitude Control for Satellites in Polar or Sun-Synchronous Orbits, J. Guid. Control. Dyn. 38 (2015) 1947–1958. doi:10.2514/1.G000751.

[38] E. Roibás-Millán, A. Alonso-Moragón, A.G. Jiménez-Mateos, S. Pindado, Testing solar panels for small-size satellites: The UPMSAT-2 mission, Meas. Sci. Technol. 28 (2017). doi:10.1088/1361-6501/aa85fc.

[39] Arianespace, Auxiliary Passengers User's Manual, (2017).